Infrared Spectra and Structures for Group 4 Dihydroxide and Tetrahydroxide Molecules

Xuefeng Wang and Lester Andrews*

Department of Chemistry, University of Virginia, McCormick Road, P.O. Box 400319, Charlottesville, Virginia 22904-4319

Hafnium and zirconium atoms react with H_2O_2 molecules and with $H_2 + O_2$ mixtures to form $M(OH)_2$ and $M(OH)_4$ molecules, which are trapped in solid argon and identified from isotopic shifts in the infrared spectra. Electronic structure calculations at the MP2 level converge to almost linear $M(OH)_2$ and tetrahedral $M(OH)_4$ molecules and predict vibrational frequencies for mixed isotopic molecules of lower symmetry that are in excellent agreement with experimental measurements, thus substantiating the identification of hafnium and zirconium dihydroxide and tetrahydroxide molecules. Titanium atoms react to give the same product molecules, but $Ti(OH)_4$ has an S_4 structure with bent Ti–O–H bonds, $Ti(OH)_2$ appears to be nearly linear, and the more stable tetravalent HM(O)OH isomer is more prominent for Ti. The Group 4 tetrahydroxides reported here are the first examples of pure metal tetrahydroxide molecules.

Introduction

The chemistry of metal hydroxides is represented by the ionic alkali and heavy alkaline earth metal compounds, which are very strong bases in aqueous solution. Although a number of trihydroxides are known, such as those of aluminum, scandium, several late-first-row transition metals, and the rare earth metals, there is no evidence for a crystalline metal tetrahydroxide compound.[1–4] No pure Group 4 transition metal hydroxides have been reported, but some zirconium and hafnium hydroxy complex sulfates and hydrates have been prepared.[2] Metal hydroxide spectroscopy in the gas phase is limited to simple monohydroxide molecules,[5–8] but we have demonstrated that group 2 and 12 $M(OH)_2$ molecules can be formed by the reaction of excited metal atoms with H_2O_2 or with $H_2 + O_2$ mixtures in excess argon and investigated by matrix IR spectroscopy.[9–11]

A tetrahydroxide molecule can, in principle, be formed by tetravalent Group 4 metal atoms. Atomic Hf and Zr are very reactive: the ground-state metal atoms insert into O_2 to make OHfO and OZrO, and the excited atoms react with H_2 to form both MH_2 and MH_4 molecules.[12–14] Furthermore, the reaction of ZrH_2 and H_2 to produce ZrH_4 is exothermic.[15] Therefore a favorable reaction between Group 4 metal atoms and H_2O_2 is expected, and a brief report on $Hf(OH)_4$ has been published.[16]

Experimental and Theoretical Methods

Laser-ablated Hf, Zr, and Ti atoms were co-deposited with H_2O_2 molecules diluted in argon during condensation onto a 10 K cesium iodide window.[12–14,17] A hydrogen peroxide complex with urea (Aldrich) at room temperature behind a Chemglass stopcock provided H_2O_2 molecules to the flowing argon reaction medium, and deuterium-substituted urea/D_2O_2 was prepared employing methods to exchange urea and H_2O_2 with D_2O as described previously.[18] Matrix infrared spectra were recorded on a Nicolet 750 spectrometer after sample deposition, after annealing, and after irradiation using a mercury arc lamp. Parallel experiments employed H_2 and O_2 mixtures in order to incorporate $^{18}O_2$ into the product molecules.[9–11]

Structures and vibrational frequencies of Group 4 $M(OH)_2$ and $M(OH)_4$ molecules were calculated using the B3LYP functional with the large 6-311++G(3df,3pd) basis set and the MP2 method with the medium 6-311++G(d,p) basis set for H, O, and Ti atoms.[19,20] Relativistic effects were accounted for in the SDD pseudopotentials for hafnium and zirconium (12 valence electrons).[21] Complementary CCSD structure calculations were done using the medium basis set. All structural parameters were varied, and the converged minimum-energy structures are stable with all real frequencies. Reaction energies given are B3LYP values, and frequencies and structures are MP2 results.

Results and Discussion

Infrared spectra of the products of Group 4 metal atom reactions with H_2O_2 and with $H_2 + O_2$ mixtures and electronic structure calculations of metal hydroxide molecules are presented below.

Hafnium. Laser-ablated Hf atoms were co-deposited with H_2O_2 in excess argon in five different experiments using a range of concentrations, annealing cycles, and irradiations. Figure 1 illustrates infrared spectra from a low H_2O_2 concentration sample where the 3470 cm^{-1} $(H_2O_2)_2$ band was one-third of the absorbance of the 3587 cm^{-1} H_2O_2 band.[18a] The stronger new 3796.2 and 666.0 cm^{-1} product bands are labeled **t** (to identify tetrahydroxide), and the much weaker 3788.6 and 660.6 cm^{-1} absorptions are marked **d** (to indicate dihydroxide). Annealing to temperatures between 20 and 45 K (in 5–6 K steps) and recooling to 10 K allowed the **t** bands to increase together by a 1.7 factor and the **d** bands by a 2.3 factor on annealing to 26–34 K, while H_2O_2 decreases and $(H_2O_2)_2$ increases. Then, **t** decreases upon higher annealing with 50% of the original **t** intensity, and **d** decreases with 20% of original intensity remaining after annealing to 45 K. In experiments with higher H_2O_2 concentrations, the **t** bands were stronger, and the **d** bands were weaker. In still another experiment, UV irradiation ($\lambda >$ 220 nm) increased the **t** bands by 50% and slightly decreased the **d** absorptions. The **t** absorptions were very sharp with full-widths at half-maximum of 0.6 and 1.5 cm^{-1}, respectively.

* To whom correspondence should be addressed. E-mail: lsa@virginia.edu.
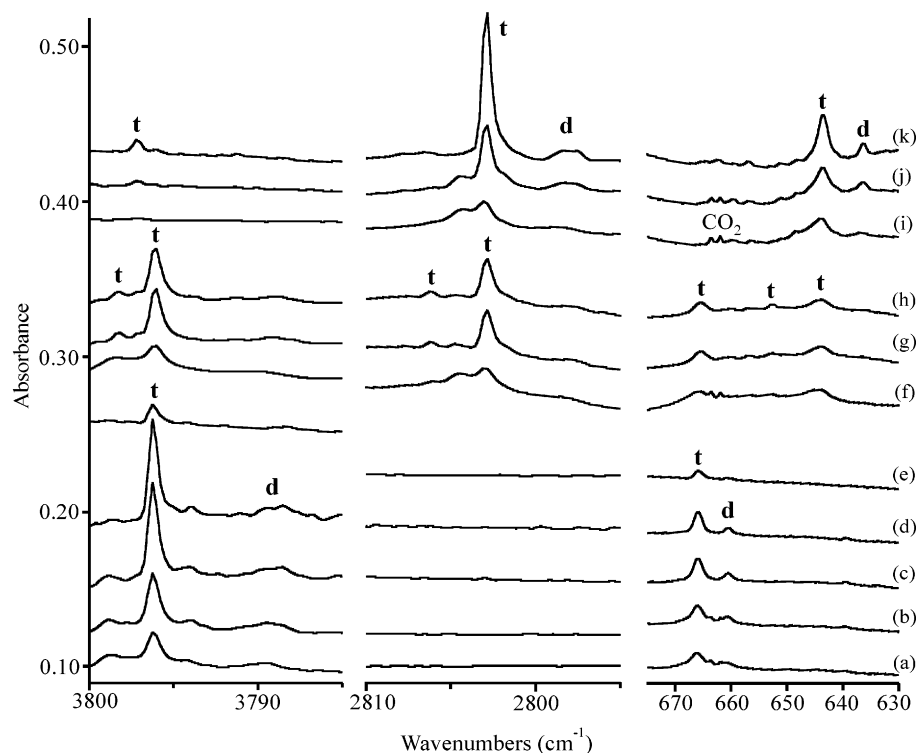
Figure 1. Infrared spectra of laser-ablated Hf atom and H_2O_2 reaction products in excess argon at 10 K. (a) H_2O_2, (b) after annealing to 20 K, (c) after annealing to 26 K, (d) after annealing to 40 K, (e) after annealing to 45 K, (f) $H_2O_2 + D_2O_2$, (g) after annealing to 26 K, (h) after annealing to 38 K, (i) D_2O_2, (j) after annealing to 24 K, and (k) after annealing to 32 K.

TABLE 1: Observed and Calculated Frequencies (cm^{-1}) for Hf(OH)$_4$ in the T_d Structure $^1A_1$ State

	Hf(OH)$_4$		Hf(OH)$_2$(OD)$_2$		Hf(OD)$_4$	
mode	obs[a]	calcd[b]	obs	calcd[c]	obs	calcd
O−H stretch		4070.0 (a_1, 0)[d]	3798.6	4067.8 (172)		2969.8 (0)
			3796.4	4065.7 (346)		
O−H stretch	3796.4	4065.7 (t_2, 345 × 3)	2806.4	2966.7 (125)	2803.0	2963.6 (248 × 3)
			2803.2	2963.6 (248)		
Hf−O stretch		695.9 (a_1, 0)	691.7	688.1 (17)		674.7 (0)
			663.6	663.6 (207)		
Hf−O stretch	666.0	663.3 (t_2, 197 × 3)	653.7	652.3 (181)	643.6	646.4 (198 × 3)
			645.6	646.5 (189)		
Hf−O−H bend		299.7 (t_2, 510 × 3)[e]		298.7 (293)		247.7 (270 × 3)
				290.6 (448)		

	Hf(^{16}OH)$_2$(^{18}OH)$_2$		Hf(^{18}OH)$_4$		Hf(^{18}OD)$_4$	
mode	obs	calcd	obs	calcd	obs	calcd
O−H stretch	3799.1	4068.1 (124)		4055.9 (0)		2949.4 (0)
	3796.4	4065.7 (345)				
O−H stretch	3786.2	4053.6 (213)	3784.4	4051.9 (330 × 3)	2785.2	2944.0 (230 × 3)
	3784.4	4051.9 (330)				
Hf−O stretch	682.2	685.1 (37)		658.3 (0)		640.4 (0)
	666.0	663.7 (197)				
Hf−O stretch	645.9	640.2 (153)	639.1	632.5 181 × 3)	617.5	617.9 (183 × 3)
Hf−O−H bend	639.1	632.6 (182)		295.7 (501 × 3)		239.6 (266 × 3)

[a] Observed **t** bands in solid argon. [b] Calculated at the MP2/6-311++G(d,p)/SDD level. [c] O−H (O−D) stretching frequencies calculated for Hf(OH)$_3$(OD): 4068.9 (86), 4065.7 (345 × 2), 2965.2 (186). O−H (O−D) stretching frequencies calculated for Hf(OH)(OD)$_3$: 4066.8 (259), 2968.3 (62), 2963.6 (248 × 2). [d] Mode symmetry in T_d, infrared intensity (km/mol). [e] Additional frequencies calculated at 297.4 (e, 0 × 2), 266.6 (t_1, 0 × 3), 183.8 (t_2, 5 × 3), and 178.7 (e, 0 × 2).

Similar investigation with D_2O_2 gave **t** absorptions at 2803.0 and 643.6 cm^{-1} and weaker **d** bands at 2797.9 and 636.5 cm^{-1}, as shown at the top of Figure 1. A weak **t** absorption at 3797.2 cm^{-1} (Figure 1k) arises from reaction with the approximately 10% HDO_2 in the D_2O_2 sample. The major product absorptions are listed in Tables 1 and 2. In addition, weak absorptions were observed for HHfO (902.7, 1626.7 cm^{-1}), DHfO (901.1, 1165.8 cm^{-1}), H_2HfO (1646.2, 921.5 cm^{-1}), H_2Hf(OH)$_2$ (1675.8,

1665.3, 690.8 cm^{-1}), and HfO_2 (813.8, 883.3 cm^{-1}) based on agreement with previous work,[12,22] and more weak new absorptions are collected in Table 3. Weak product absorptions common to laser-ablation experiments due to the H_2O−HO radical complex and the HO_2(DO_2) and OH(OD) radicals were also observed.[23−25]

Simultaneous co-deposition of Ar/H_2O_2 and Ar/D_2O_2 streams with Hf atoms showed no evidence of isotopic exchange in the

TABLE 2: Observed and Calculated Frequencies (cm^{-1}) for Hf(OH)$_2$ in the C_{2v} Structure

| | Hf(OH)$_2$ | | Hf(OH)(O D) | | Hf(OD)$_2$ | |
mode	obs[a]	calcd[b]	obs	calcd	obs	calcd
O−H stretch		4030.9 (a$_1$, 9)[c]	3789.0	4031.1 (242)		2940.2 (5)
O−H stretch	3788.8	4031.2 (b$_2$, 474)	2799.4	2939.5 (171)	2797.9	2938.7 (337)
Hf−O stretch		702.9 (a$_1$, 0)		694.5 (14)		681.7 (0)
Hf−O stretch	660.6	661.6 (b$_2$, 244)	649.4	651.6 (225)	636.5	645.4 (232)
Hf−O−H bend		507.7 (b$_2$, 13)	488.7	495.8 (92)		380.6 (6)
Hf−O−H bend		494.1 (a$_2$, 0)	−	487.5 (95)		378.2 (96)
Hf−O−H bend		483.2 (a$_1$, 184)		378.6 (55)		376.9 (92)
Hf−O−H bend	471.4	481.2 (b$_1$, 191)		374.5 (48)		370.2 (92)
O−Hf−O bend		51.3 (a$_1$, 13)		49.0 (12)		46.7 (11)

| | Hf(^{16}OH)(^{18}OH) | | Hf(^{18}OH)$_2$ | | Hf(^{18}OD)$_2$ | |
mode	obs	calcd	obs	calcd	obs	calcd
O−H stretch	3788.8	4031.1 (248)		4017.1 (9)		2920.2 (5)
O−H stretch	3776.7	4017.3 (226)	3776. 7	4017.6 (454)	2779. 7	2919.2 (213)
Hf−O stretch		690.5 (35)		664.9 (0)		647.1 (0)
Hf−O stretch	643.0	640.6 (199)	635.6	632.3 (223)	607.2	618.1 (214)
Hf−O−H bend		506.1 (15)		504.1 (14)		375.9 (6)
Hf−O−H bend		492.8 (4)		490.8 (0)		370.5 (95)
Hf−O−H bend		480.3 (182)		477.7 (184)		369.7 (92)
Hf−O−H bend		477.8 (186)	467.1	475.2 (191)		365.7 (0)
O−Hf−O bend		50.4 (12)		49.4 (12)		45.4 (11)

[a] Observed **d** bands in solid argon. [b] Calculated at the MP2/6-311++G(d,p)/SDD level. [c] Mode symmetry in C_{2v}, infrared intensity (km/mol).

TABLE 3: Additional Minor Product Absorptions in Group 4 Metal Atom Reactions with H$_2$O$_2$ and H$_2$ + O$_2$

Hf, H$_2$O$_2$, H$_2$ + O$_2$	Zr, H$_2$O$_2$	Zr, D$_2$O$_2$	Ti, H$_2$O$_2$	Ti, D$_2$O$_2$
3889.6	3721.5		3751.2	2771.6
3782.2	1539.6	1108.7	1689.9	
888.1				
728.8	896.9	896.5	1681.5	
718.0	701.7		822.8	797.4
708.0	635.7	622.4	822.0	819.4
639.6			776.4	
622.2			699.5	
			677.0	666.8

reagent spectra. The major new product bands were observed at 3796.2 cm^{-1} with a 3799.0 cm^{-1} shoulder and 2803.0 cm^{-1} with a 2804.5 cm^{-1} shoulder on deposition. As in the pure H$_2$O$_2$ and D$_2$O$_2$ samples, annealing increased the major product 3796.2 and 2803.0 cm^{-1} bands and decreased the shoulders, but with the H$_2$O$_2$ + D$_2$O$_2$ mixture, new satellite features were observed at 3798.3 and 2806.2 cm^{-1} above each major band, and the **d** bands appeared at 3788.6 and 2797.9 cm^{-1}. The lower-frequency region revealed **t** bands at 665.6, 653.0, and 643.8 cm^{-1} and a weak **d** band at 657.1 cm^{-1}, as shown in Figure 1f–h.

Next, experiments were performed with Hf and H$_2$ or D$_2$ + O$_2$ as reaction partners, and the resulting infrared spectra for isotopic samples are shown in Figure 2. The **t** bands appeared at 3796.4 and 666.0 cm^{-1} with 3-fold weaker intensity, but the **d** bands were comparable. As expected, the HfO$_2$ absorptions were also stronger, but HfH$_2$ was weak at 1622.4 cm^{-1}, and HfH$_4$ was strong at 1678.5 and 1675.7 cm^{-1}.[14] Two minor 3777.5 and 3775.1 cm^{-1} bands were stronger, and weak additional 728.8, 718.0, and 708.0 cm^{-1} bands were recorded. The product bands shifted to 2803.2 and 643.6 cm^{-1} with D$_2$ and when ^{16}O$_2$ was replaced by ^{18}O$_2$, and additional important isotopic splittings were observed with the H$_2$ + ^{16}O$_2$ + ^{16}O^{18}O + ^{18}O$_2$ and the HD + O$_2$ reagent mixtures.

The sharp major product **t** absorptions at 3796.4 and 666.0 cm^{-1} are grouped together by parallel increases and decreases upon annealing (Figure 1a–e), and these absorptions are characterized as O−H and Hf−O stretching modes by the effect of isotopic substitution. First, the 3796.4 cm^{-1} band shifts to 2803.0 cm^{-1} with deuterium (the characteristic H/D isotopic frequency ratio is 1.3544) and to 3784.4 cm^{-1} with oxygen-18 (the ^{16}O/^{18}O isotopic frequency ratio is 1.00317), which precisely match an O−H stretching mode.[9−11] Second, the 666.0 cm^{-1} absorption shifts to 639.1 cm^{-1} with oxygen-18 (^{16}O/^{18}O ratio = 1.03933), which is lower than that observed for the antisymmetric Hf−O stretching mode in HfO$_2$ (ratio = 1.05345).[12] Finally, the deuterium shift to 643.6 cm^{-1} shows that the H and D atoms also participate in this normal mode.

Mixed isotopic spectra clearly identify the molecular stoichiometry of the new reaction products. The ^{16}O$_2$ + ^{16}O^{18}O + ^{18}O$_2$ mixed isotopic reagent produced the same major **t** bands as ^{16}O$_2$ and ^{18}O$_2$ separately with H$_2$, plus weak new bands at 3799.1, 3797.9, 3787.3, 3786.2, and 3785.2 cm^{-1} in the O−H stretching region and at 684.8, 682.2, 676.7, 651.8, and 645.9 cm^{-1} in the Hf−O stretching region for mixed isotopic molecules. Reaction with HD and ^{16}O$_2$ shifted the major bands slightly to 3796.3 and 2803.2 cm^{-1} and weak new peaks to 3799.7, 3798.6, 3797.2 (shoulder), 2808.1, 2806.4, and 2804.8 cm^{-1} in the upper region. The weak 3797.2 cm^{-1} product from HDO$_2$ in the D$_2$O$_2$ sample was observed as a shoulder with HD + O$_2$, and major bands appeared at 667.6 and 645.6 cm^{-1} and weak peaks at 695.2, 691.7, 682.8, 663.6, 649.4, and 643.7 cm^{-1} in the lower region.

The straightforward reaction product Hf(OH)$_4$ was computed using the MP2 and B3LYP methods. The Hf reaction with two H$_2$O$_2$ molecules is strongly exothermic and spontaneous in the cold matrix, and Hf(OH)$_4$ is a very stable molecule. The converged tetrahedral structure is depicted in Figure 3, and the frequencies are listed in Table 1 as computed at the MP2 level. Complementary CCSD calculations were performed under S_4 symmetry, but it was not possible to attain convergence, as the potential energy surface for the Hf−O−H angles is nearly flat. The Hf−O−H bond angle varies between 167° and 174° as the calculation proceeds (Hf−O, 1.952 Å; O−H, 0.948 Å). Our B3LYP calculation converges to an S_4 structure with more bent 154° Hf−O−H valence angles; 1.957 and 0.952 Å bond lengths; O−H stretching modes at 3987.0 cm^{-1} (e, 2 × 261 km/mol,
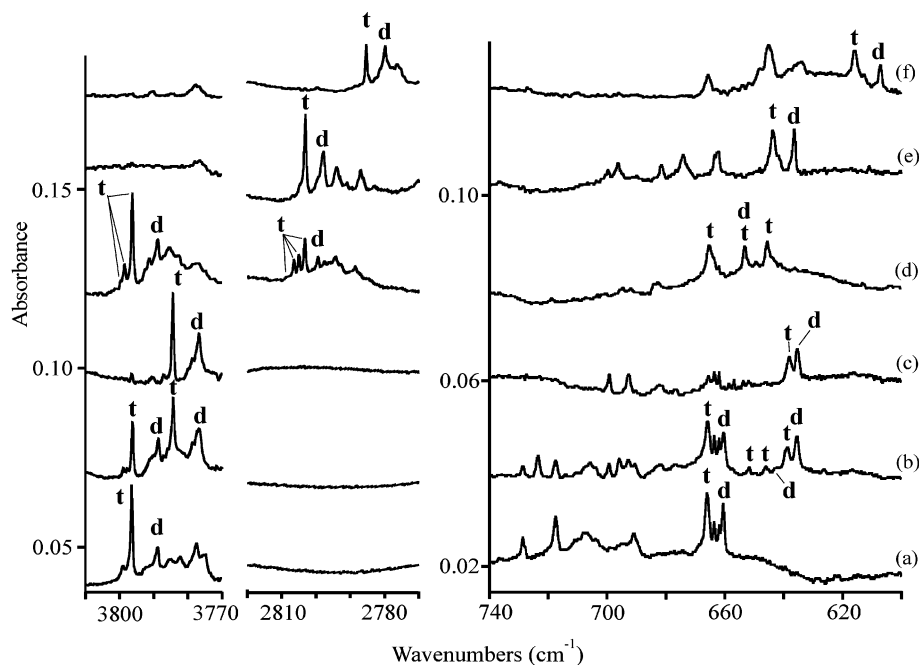
Figure 2. Infrared spectra of Hf and $H_2 + O_2$ reaction products in excess argon at 10 K after full-arc irradiation and annealing to 24−30 K. (a) $H_2 + {}^{16}O_2$, (b) $H_2 + {}^{16}O_2 + {}^{16}O{}^{18}O + {}^{18}O_2$, (c) $H_2 + {}^{18}O_2$, (d) HD + ${}^{16}O_2$, (e) $D_2 + {}^{16}O_2$, and (f) $D_2 + {}^{18}O_2$.
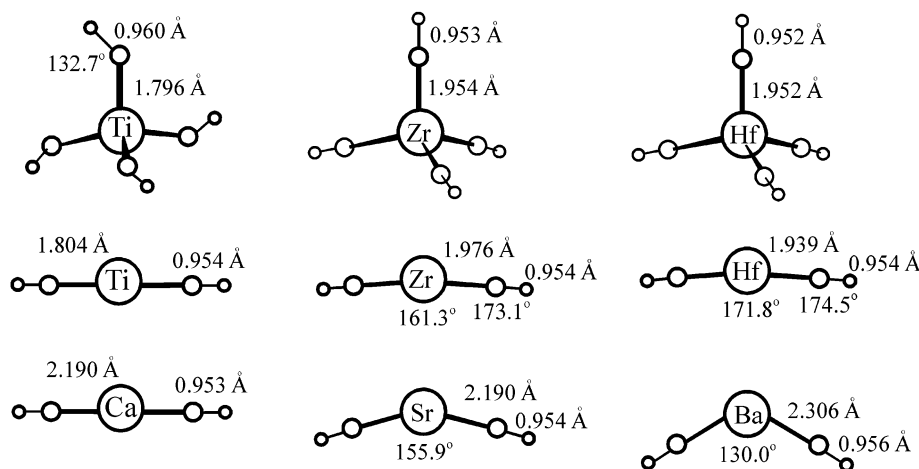
Figure 3. Structures converged for the Group 4 M(OH)$_4$ and M(OH)$_2$ molecules at the MP2 level [6-311++G(d,p) for H, C, and TI and SDD for Zr and Hf]. The structures for group 2 dihydroxides are taken from ref 10.

doubly degenerate mode, intensity 261 km/mol for each component), 3987.1 cm^{-1} (b, 216 km/mol), and 3991.8 cm^{-1} (a, 0 km/mol); and Hf−O stretching modes at 686.2 cm^{-1} (a, 0 km/mol), 659.5 cm^{-1} (b, 146 km/mol), and 656.8 cm^{-1} (e, 2 × 176 km/mol). Because the **t** bands are sharp (0.6 and 1.5 cm^{-1} bandwidths), a computed 2.7 cm^{-1} band splitting for the Hf−O stretching mode can be eliminated, and the higher-symmetry tetrahedral structure is favored. However, a very slight bending of the Hf−O−H angles is not likely to affect the matrix absorptions and cannot be ruled out.

$$\text{Hf}\,(^3\text{F}) + 2\text{H}_2\text{O}_2 \xrightarrow{\text{relax}} \text{Hf(OH)}_4 \qquad (\Delta E = -400 \text{ kcal/mol})$$
$$(1)$$
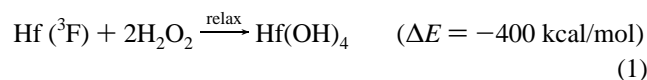
Excellent agreement is found between calculated and observed frequencies. The MP2 method typically overestimates observed frequencies,[26] and a like calculation for H_2O_2 provides a calibration scale factor, which is expressed as observed/calculated frequency = 3588/3848 = 0.932. This scale factor multiplied by our MP2-calculated antisymmetric O−H stretching frequency for Hf(OH)$_4$ gives a 3791 cm^{-1} absorption, which is close to the observed 3796.4 cm^{-1} band. The antisymmetric Hf−O stretching mode computed at 663.3 cm^{-1} is observed at 666.0 cm^{-1}. In addition, the MP2 calculation predicts 16.9 and 30.8 cm^{-1} D and ^{18}O shifts, and we observe 22.4 and 26.9 cm^{-1} isotopic shifts for this mostly antisymmetric O−Hf−O stretching mode, which is slightly more D and less O character than calculated at the MP2 level of theory.

The best experimental evidence we have for the tetrahydroxide identification of the major product species is observation of the new Hf(OH)$_2$(OD)$_2$ isotopic modification in addition to Hf(OH)$_4$ and Hf(OD)$_4$ using $H_2O_2 + D_2O_2$ as the reagent. The Hf(OH)$_2$(OD)$_2$ molecule has C_{2v} symmetry, and all four O−H(O−D) and Hf−OH(Hf−O-D) stretching modes are observable. We observe these bands with the predicted shifts relative to T_d symmetry: Hf(OH)$_4$ and Hf(OD)$_4$ (Table 1). The antisymmetric O−H and O−D stretching modes are unshifted from the Hf(OH)$_4$ and Hf(OD)$_4$ values, but the symmetric O−H and O−D stretching modes are observed as new bands at 3798.3 and 2806.2 cm^{-1}, respectively. The HD + O$_2$ experiment in

addition gives $Hf(OH)_3(OD)$ and $Hf(OH)(OD)_3$ at 3799.7, 2804.9 cm^{-1} and 3797.2, 2808.1 cm^{-1} in the upper region and at 695.2, 663.6, 649.4 cm^{-1} and 682.8, 643.7 cm^{-1}, respectively, in the lower region. With the mixed $^{16}O_2 + ^{16}O^{18}O + ^{18}O_2$ precursor, the five $Hf(^{16}OH)_{n-4}(^{18}OH)_n$ ($n = 0-4$) product molecules are observed, as shown by calculated frequency shifts. The major $Hf(^{16}OH)_2(^{18}OH)_2$ species exhibits stronger new peaks at 3799.1 and 3786.2 cm^{-1} in the upper region and at 645.9 cm^{-1} in the lower region. However, with the $H_2O_2 + D_2O_2$ precursor, only three tetrahydroxide products are possible, namely, $Hf(OH)_4$, $Hf(OH)_2(OD)_2$, and $Hf(OD)_4$, and absorptions for these isotopic molecules are dominant. The former two absorb strongly at 3796.2 cm^{-1} (antisymmetric O−H stretch), but only the mixed isotopic molecule absorbs at 3798.3 and 2806.2 cm^{-1} (symmetric O−H and O−D stretches), and the latter two absorb strongly at 2803.0 cm^{-1} (antisymmetric O−D stretch). Likewise, the $Hf(OH)_2(OD)_2$ molecule shares the stronger 665.6 and 643.8 cm^{-1} absorptions, but alone accounts for the 653.0 cm^{-1} band (Table 1). The excellent agreement found here between observed and calculated frequencies for Hf-$(OH)_4$, including the mixed H, D and ^{16}O, ^{18}O isotopic modifications of lower symmetry, confirms our identification of $Hf(OH)_4$ and provides the first conclusive evidence for a metal tetrahydroxide molecule.[16]

The O−H and O−D stretching mode coupling in the $Hf(OH)_{n-4}(OD)_n$ ($n = 0-4$) molecules is a textbook example, and we start with one active t_2 mode for $Hf(OH)_4$ at 3796.4 cm^{-1} and one for $Hf(OD)_4$ at 2803.2 cm^{-1}. For the trigonal mixed isotopic molecules, the e modes are the same frequency as the above t_2 modes, and the a_1 modes of the trigonal subunits couple differently and are observed 3.4 and 4.9 cm^{-1} higher, respectively (calculated 3.2 and 4.7 cm^{-1} higher), but the a_1 modes of the lone O−H and O−D subunits are uncoupled and are observed only 0.9 and 1.6 cm^{-1} higher, respectively (calculated 1.1 and 1.6 cm^{-1} higher). For the $Hf(OH)_2(OD)_2$ molecules, the symmetric O−H and O−D stretching modes are observed 2.2 and 3.2 cm^{-1} higher than the antisymmetric counterparts, respectively (calculated 2.1 and 3.1 cm^{-1} higher), and the antisymmetric modes coincide with the above e and t_2 modes. (See Figure 6 below for the Zr system.)

Judging from our calculations and the sharp matrix absorptions for $Hf(OH)_4$, we believe that the structure is nearly tetrahedral. Our B3LYP calculation for $Hf(OH)_2(OD)_2$ predicts 2.3/2.5 and 2.9/3.0 cm^{-1} separations between the symmetric and antisymmetric O−H/O−D stretching modes, which is outside the observed 2.2 and 3.2 cm^{-1} separations; hence, the Hf−O−H angle is more nearly linear than the 154° value computed at the B3LYP level.

The weaker **d** bands appear in the same regions, and these bands are favored with lower H_2O_2 concentration and in the reaction with $H_2 + O_2$ samples. The MP2 calculation for Hf-$(OH)_2$ predicts 34.5 and 1.7 cm^{-1} lower O−H and Hf−O stretching frequencies, respectively, and the **d** bands are observed 7.6 and 5.4 cm^{-1} lower (Table 2). The nearly linear structure for $Hf(OH)_2$ is similar to the structures computed for the highly ionic $Ca(OH)_2$ and $Sr(OH)_2$ molecules (Figure 3).[9,10,27] Note that both O−H and O−D stretching modes, one Hf−O stretching mode, and a Hf−O−H bending mode are observed for the lower-symmetry $Hf(OH)(OD)$ molecule, which are in excellent agreement with calculations. The O−H stretching modes for $Hf(^{16}OH)(^{18}OH)$ are unshifted from the $Hf(^{16}OH)_2$ and $Hf(^{18}OH)_2$ values, and the Hf−O stretching mode at 643.0 cm^{-1} is in the relative position predicted by calculations. Therefore, the **d** bands can be assigned to $Hf(OH)_2$.

The $Hf(OH)_2$ molecule has a computed stable, nearly linear $^1A_1$ ground state, and reaction 2 is exothermic and spontaneous in the matrix, based on the growth of **d** absorptions observed upon annealing. [The B3LYP calculation predicts a similar ground-state structure (O−Hf−O angle, 154.8°; Hf−O−H angle, 162.1°; Hf−O, 1.932 Å; O−H, 0.953 Å) and b_2 frequencies (3978.6 and 672.6 cm^{-1}). A nearly linear $^3B_1$ state is 21 kcal/mol (MP2) or 12 kcal/mol (B3LYP) higher in energy, and another singlet excited state is 88 kcal/mol (MP2) above the ground state.] The HfO_2 absorptions do not increase upon this annealing, which suggests that $Hf(OH)_2$ and $Hf(OH)_4$ are stable molecules under matrix isolation conditions. However, fast relaxation of the energized $Hf(OH)_2$ product is required for its stabilization in the matrix. In contrast, gas-phase metal atom reactions with H_2O_2 give the MOH monohydroxide.[6]

$$Hf\,(^3F) + H_2O_2 \rightarrow Hf(OH)_2\,(^1A_1)$$
$$(\Delta E = -203 \text{ kcal/mol})\ (2)$$
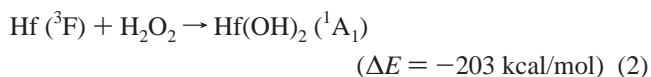
We note the parallel observations for stronger HfH_4 absorptions relative to HfH_2 in H_2 reactions and stronger $Hf(OH)_4$ bands relative to $Hf(OH)_2$ in H_2O_2 reactions. This underscores the favorable reaction to form the tetravalent hafnium species.

Supporting evidence for these observations is found in the Hf/H_2O experiments of Zhou et al.,[22] who observed our **t** and **d** absorptions upon annealing after mercury arc photolysis. However, the relative intensities were reversed in the Hf/H_2O experiments, and the 3788.5 and 660.6 cm^{-1} bands appeared first upon 30 K annealing and increased upon 35 K annealing, when the 3796.1 and 665.8 cm^{-1} bands appeared. The formation of $Hf(OH)_2$ is not as straightforward in the H_2O experiments and in our $H_2 + O_2$ reactions where the final reaction to form $Hf(OH)_4$ is even more complicated, and accordingly, the yield is lower. However, the UV irradiation that increases the yield of $Hf(OH)_4$ in $Hf + H_2 + O_2$ experiments also produces the H_2O−HO radical complex, which shows that OH radicals are formed and that the direct synthesis of metal hydroxide species follows accordingly. On the other hand, on the basis of the marked growth of $Hf(OH)_4$ upon annealing in our H_2O_2 experiments, reaction 3 appears to be spontaneous. We note the parallel observations of stronger HfH_4 absorptions relative to HfH_2 in H_2 reactions and stronger $Hf(OH)_4$ bands relative to $Hf(OH)_2$ in H_2O_2 reactions. This substantiates the favorable reactions to form the tetravalent hafnium species.

$$Hf(OH)_2 + H_2O_2 \rightarrow Hf(OH)_4 \qquad \Delta E = -197 \text{ kcal/mol}\ (3)$$
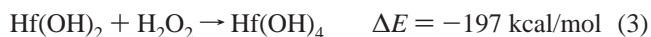
The singlet tetravalent HHf(O)OH isomer is computed to be 1 kcal/mol (MP2) or 3 kcal/mol (B3LYP) more stable than the $^1A_1$ ground-state $Hf(OH)_2$ molecule, and this isomer must be considered for some of the remaining weak absorptions (Table 3). Two of these at 888.1 and 639.6 cm^{-1} with H_2O_2 increase upon annealing roughly following the **d** bands, but they are unaffected by UV irradiation whereas the **d** bands are reduced. These modes are predicted at 906.3 and 665.3 cm^{-1} at the B3LYP level of theory. These bands shift with D_2O_2 to 887.3 and 622.8 cm^{-1}, which are appropriate for terminal Hf=O and Hf−OH stretching modes. The Hf−H stretching region is complicated with H_2O, and no associated band can be found. The 888.1 and 639.6 cm^{-1} bands are tentatively assigned to the isomer HHf(O)OH.

The simple HfOH monohydroxide molecule is not observed, but the 21 kcal/mol more stable H−Hf=O isomer[22] is formed in low yield upon sample deposition with the H_2O_2 and $H_2 + O_2$ reagents. With slow matrix relaxation, the reaction 2 product

**TABLE 4: Observed and Calculated Frequencies (cm^{-1}) for Zr(OH)$_4$ in the T_d Structure $^1A_1$ State**

mode	Zr(OH)$_4$		Zr(OH)$_2$(OD)$_2$		Zr(OD)$_4$	
	obs[a]	calcd[b]	obs	calcd[c]	obs	calcd
O−H stretch		4053.1 (a$_1$, 0)[d]	3785.0	4050.6 (182)		2957.4 (0)
			3782.6	4048.1 (366)		
O−H stretch	378 2.6	4048.1 (t$_2$, 366 × 3)	2796.0	2953.9 (133)	2792.6	2950.4 (2 64 × 3)
			2792.9	2950.4 (264)		
Zr−O stretch		692.5 (a$_1$, 0)		689.9 (122)		671.3 (0)
			677.5	687.4 (280)		
Zr−O stretch	681. 6,	690.8 (t$_2$, 297 × 3)	659.3	671.6 (263)	658.8	671.6 (26 8 × 3)
	680. 5			671.5 (149)		
Zr−O−H bend		289.7 (t$_2$, 485 × 3)[e]				250.7 (234 × 3)

mode	Zr(^{16}OH)$_2$(^{18}OH)$_2$		Zr(^{18}OH)$_4$	
	obs	calcd	obs	calcd
O−H stretch	3785.5	4051.0 (125)		4039.1 (0)
	3782.6	4048.1 (366)		
O−H stretch	3772.2	4036.4 (233)	3770.7	4034.5 (350 × 3)
	3770.7	4034.5 (350)		
Zr−O stretch		689.8 (134)		655.0 (0)
	680	687.4 (273)		
Zr−O stretch	651	658.8 (257)	651.1	658.7 (256 × 3)
		657.1 (131)		
Zr−O−H bend				284.0 (484 × 3)

[a] Observed **t** bands in solid argon. [b] Calculated at the MP2/6-311++G(d,p)/SDD level. [c] O−H (O−D) stretching frequencies calculated for Zr(OH)$_3$(OD): 4051.9 (91), 4048.1 (366 × 2), 2952.2 (198). O−H (O−D) stretching frequencies calculated for Zr(OH)(OD)$_3$: 4049.4 (274), 2955.7 (67), 2950.4 (264 × 2). [d] Mode symmetry in T_d, infrared intensity (km/mol). [e] Additional frequencies calculated at 218.9 (e, 0 × 2), 187.0 (t$_2$, 32 × 3), 181.1 (t$_1$, 0 × 3), and 183.2 (e, 0 × 2).

Hf(OH)$_2$ can lead to a small amount of the stable HHfO fragment.

$$[Hf(OH)_2]^* \rightarrow [HfOH]^* + OH \rightarrow HHfO + OH \quad (4)$$
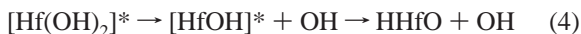
The structures of Hf(OH)$_4$ and Hf(OH)$_2$ are of considerable interest (Figure 3). At the MP2 level, the M−O−H bonds are all linear for the former T_d structure and nearly linear for the latter C_{2v} structure, which indicates a high degree of ionic bonding,[7,28] although the O−H stretching frequencies [3796 and 3788 cm^{-1} for the Hf compounds and 3724 cm^{-1} for Ba(OH)$_2$][10] do not reach the gaseous OH$^-$ value (3556 cm^{-1}).[29] The Mulliken charges (Table 4) suggest more ionic character for Ba(OH)$_2$ than for Hf(OH)$_2$ as expected from the first ionization energies (120 kcal/mol for Ba and 161 kcal/mol for Hf after the effect of lanthanide contraction).[1] The larger charge on Hf in the tetrahydroxide compared to the dihydroxide is needed to support four negatively charged OH subunits in the stable Hf-(OH)$_4$ molecule.

The pure crystalline solid Hf(OH)$_4$ does not appear to have been prepared even though the molecule is very stable. Reaction 5 is sufficiently endothermic that Hf(OH)$_4$ is unlikely to dehydrate in the gas phase. However, HfO$_2$ is a very stable refractory solid, and the stability of solid HfO$_2$ through saturation by coordination and oligomerization will probably support decomposition of Hf(OH)$_4$ in the solid phase. Heats of formation for HfO$_2$(solid) (−274 kcal/mol) and for Hf(gas) atoms (148 kcal/mol)[30] and our computed energy for HfO$_2$(g) together give an approximate heat of condensation of HfO$_2$ as −240 kcal/mol. Therefore, Hf(OH)$_4$ will probably be thermodynamically unstable in the solid phase.
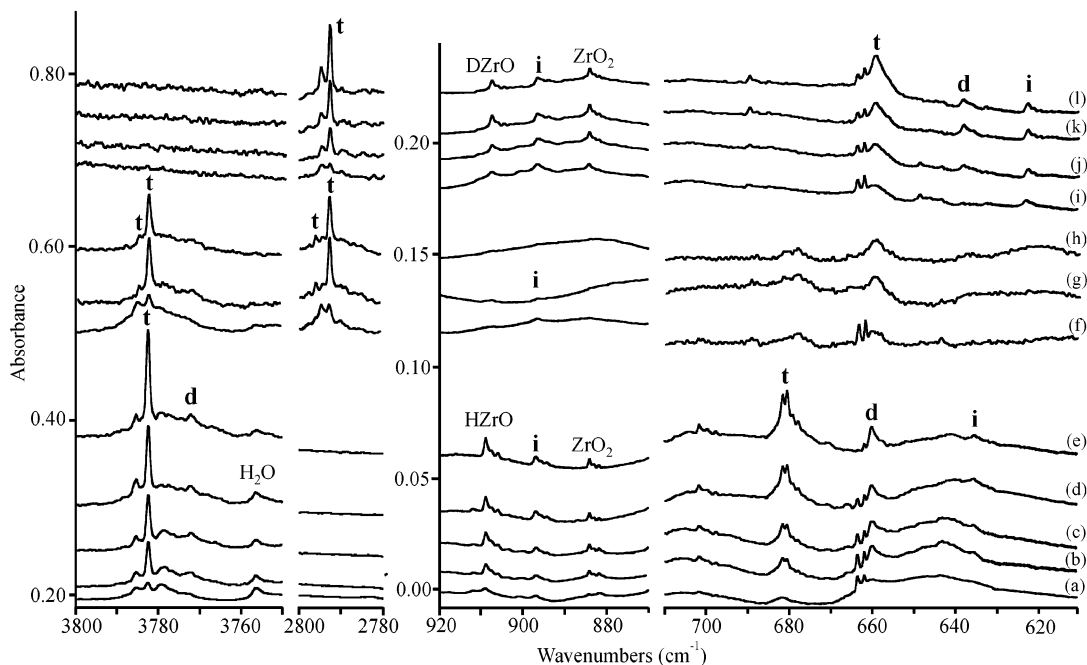
$$Hf(OH)_4 \rightarrow HfO_2 + 2H_2O \quad (\Delta E = 162 \text{ kcal/mol}) \quad (5)$$

The next most likely molecule, H$_2$Hf(OH)$_2$, has been identified in recent water experiments,[22] but there are problems with some of the assignments. Our MP2 and B3LYP calculations predict both O−H modes to be 2−4 or 5−7 cm^{-1} higher than

the strong mode for Hf(OH)$_2$, two strong Hf−H$_2$ stretching modes separated by 28−30 cm^{-1}, and two strong Hf−O stretching modes separated by 3 cm^{-1}, which are in accord with calculated frequencies presented by Zhou et al. However, our experiments show that the 690.8 and 660.6 cm^{-1} bands do not track and cannot be due to the same species. We have already assigned the 660.6 cm^{-1} band to Hf(OH)$_2$. The split 689.4 cm^{-1} part of the 690.8 cm^{-1} band is probably due to the other Hf−O stretching mode. Furthermore, the strongest computed absorption is the b$_1$ Hf−H$_2$ stretching mode, and the 1665.3 cm^{-1} band is weak enough in our experiment for the weaker O−H stretching modes expected near 3790 cm^{-1} not to be observed. In addition, the 1675.7 cm^{-1} band does not track with the 1665.3 cm^{-1} band, but a weaker 1673.3 cm^{-1} band does track the latter. The 1675.7 cm^{-1} band is probably a matrix site splitting for HfH$_4$. The 3789.6 cm^{-1} shoulder on our 3788.8 cm^{-1} Hf(OH)$_2$ band could be due to H$_2$Hf(OH)$_2$.

Zirconium. A similar series of experiments was performed with zirconium, and infrared spectra from the peroxide reactions are shown in Figure 4. The analogous **t** and **d** absorptions are observed at 3782.4, 681.6, 680.5 cm^{-1} and 3772.0, 660.2 cm^{-1} in the hydrogen systems and at 2792.6, 658.8 cm^{-1} and 2784, 638.0 cm^{-1} in the deuterium systems, respectively. The absorptions shifted with ^{18}O$_2$, and new weak satellites were observed at 3785.5, 3784.4 cm^{-1} and at 3773.4, 3777.2 cm^{-1} on the strong **t** bands with the ^{16}O$_2$ + ^{16}O^{18}O +^{18}O$_2$ mixture. In addition, sharp absorptions were also observed for ZrO$_2$ (884.2, 817.9 cm^{-1}), HZrO (1545.2, 908.8 cm^{-1}), and DZrO (1110.1, 907.4 cm^{-1}).[12,22] As observed for Hf, annealing to allow diffusion and reaction of Zr atoms increased the **t** and **d** product absorptions. Further annealing to 35 and 40 K in another experiment with comparable product yields increased **t** and **d** absorptions slightly, but annealing to 42 K reduced **t** bands by one-half, removed the **d** bands, and produced broad (H$_2$O$_2$)$_n$ absorptions.

An experiment was performed with Zr, H$_2$O$_2$, and D$_2$O$_2$ in the same matrix, and the spectra are also shown in Figure 4. The deposited sample exhibits the **t** band at 3782.4 and 2792.6

Spectra and Structures for Group 4 Di- and Tetrahydroxides

J. Phys. Chem. A, Vol. 109, No. 47, 2005 **10695**

Figure 4. Infrared spectra of Zr atom and H_2O_2 reaction products in excess argon at 10 K. (a) H_2O_2, (b) after annealing to 22 K, (c) after annealing to 26 K, (d) after $\lambda > 220$ nm irradiation, (e) after annealing to 30 K, (f) $H_2O_2 + D_2O_2$, (g) after annealing to 38 K, (h) after annealing to 40 K, (i) D_2O_2, (j) after annealing to 22 K, (k) after annealing to 24 K, and (l) after annealing to 28 K.
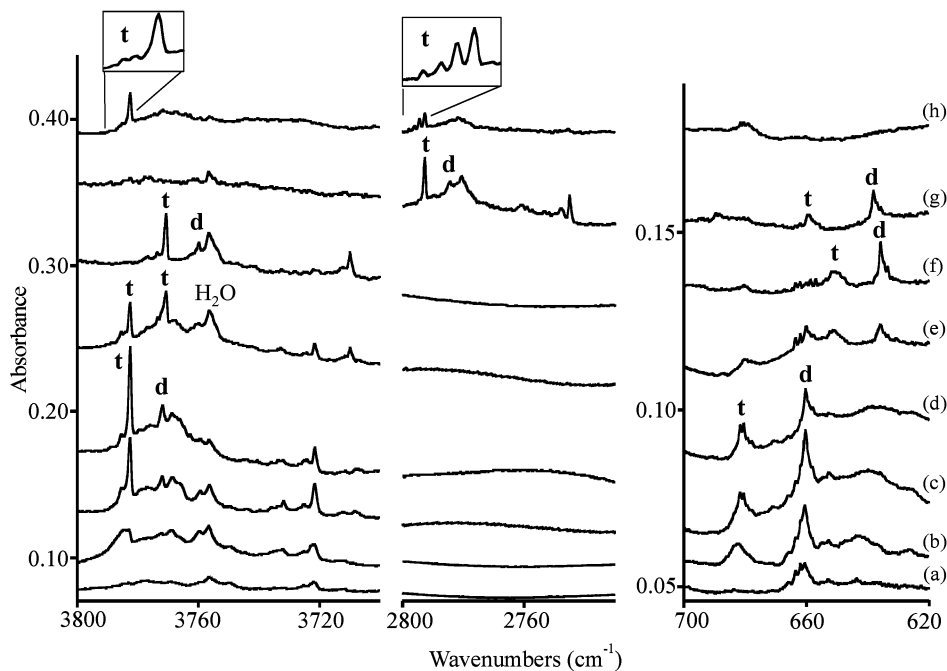
Figure 5. Infrared spectra of the Zr atom and $H_2 + O_2$ reaction products in excess argon at 10 K. (a) $H_2 + {}^{16}O_2$ deposited, (b) after $\lambda > 220$ nm irradiation, (c) after annealing to 19 K, and (d) after annealing to 24 K and infrared spectra of the following isotopic systems after irradiation and annealing to 22, 23, 28, and 26 K, respectively, (e) $H_2 + {}^{16}O_2 + {}^{16}O^{18}O + {}^{18}O_2$, (f) $H_2 + {}^{18}O_2$, (g) $D_2 + {}^{16}O_2$, and (h) $H_2 + D_2 + {}^{16}O_2$.

cm^{-1}, with matrix-effect bands at 3785.3 and 2794.6 cm^{-1}. Annealing increased the major **t** bands, decreased the matrix-effect bands, and increased new satellite absorptions at 3784.8 and 2796.0 cm^{-1}. Absorptions were observed at 681.5, 628.0, and 659.3 cm^{-1} in the lower region. The **d** absorptions were too weak to be detected.

Zirconium atoms were also reacted with $H_2 + O_2$ isotopic mixtures, and the resulting spectra are compared in Figure 5. The yields of **d** increased and **t** decreased relative to the peroxide systems, as found with hafnium. The frequencies are the same

except for the upper bands, which are at 3782.6 and 3771.8 cm^{-1}. The new product absorptions are listed in Tables 4 and 5.

The strong **t** absorption at 3782.6 shifts to 3770.7 cm^{-1} with ${}^{18}O_2$ (${}^{16}O/{}^{18}O$ frequency ratio = 1.00316) and to 2792.6 cm^{-1} with D_2 (H/D frequency ratio = 1.3544), which again characterizes an O−H stretching mode. The split 681.5, 680.4 cm^{-1} band shifts to 651.1 cm^{-1} with ${}^{18}O_2$ (${}^{16}O/{}^{18}O$ ratio = 1.0460), which is slightly less than the ratio for the antisymmetric stretching mode of ZrO_2 (1.0480). The small deuterium shift to 658.8 cm^{-1}

TABLE 5: Observed and Calculated Frequencies (cm⁻¹) for Zr(OH)₂ in the ³B₁ State

mode	Zr(OH)₂ obs[a]	Zr(OH)₂ calcd[b]	Zr(OH)(OD) obs	Zr(OH)(OD) calcd	Zr(OD)₂ obs	Zr(OD)₂ calcd	Zr(¹⁸OH)₂ obs	Zr(¹⁸OH)₂ calcd
O–H stretch		4024.3 (a₁, 30)[c]		4024.3 (204)		2934.0 (20)		4010.6 (29)
O–H stretch	3771.8	4024.3 (b₂, 377)		2933.4 (150)	2784.5	2932.8 (280)	3759.8	4010.8 (359)
Zr–O stretch	660.3	660.7 (b₂, 304)		657.5 (245)	638.0	646.1 (295)	635.7	634.9 (279)
Zr–O stretch		650.6 (a₁, 6)		637.0 (60)		631.6 (5)		615.8 (6)
Zr–O–H bend		493.9 (b₂, 27)		487.2 (101)		370.1 (12)		490.5 (28)
Zr–O–H bend		480.2 (a₁, 183)		462.9 (95)		366.8 (96)		476.0 (181)
Zr–O–H bend		464.6 (a₂, 0)		368.3 (58)		355.0 (96)		461.5 (0)
Zr–O–H bend		461.2 (b₁, 186)		351.5 (46)		347.8 (0)		456.8 (186)
O–Zr–O bend		58.8 (a₁, 5)		56.8 (4)		54.9 (4)		56.8 (4)

[a] Observed **d** bands in solid argon. [b] Calculated at the MP2/6-311++G(d,p)/SDD level. [c] Mode symmetry in C_{2v}, infrared intensity (km/mol).

evidences some H(D) participation in this normal mode. The **t** bands are assigned to Zr(OH)₄. Our MP2 calculation predicts these modes 17.1 cm⁻¹ lower and 27.5 cm⁻¹ higher than their Hf(OH)₄ counterparts, and we observe them 13.8 cm⁻¹ lower and 15.6 cm⁻¹ higher, respectively. The strong 3782.6 cm⁻¹ absorption is sharp (1.0 cm⁻¹ full-width at half-maximum), but the 681.6 cm⁻¹ band exhibits a 680.5 cm⁻¹ splitting. The tetrahedral structure calculated for singlet Zr(OH)₄ is illustrated in Figure 3. We cannot determine whether distortion from tetrahedral symmetry occurs for Zr(OH)₄ in the solid argon matrix, but slightly bent Zr–O–H angles cannot be ruled out. In this regard, our B3LYP calculation converges to an S_4-symmetric molecule with Zr–O and O–H bond distances of 1.963 and 0.954 Å and Zr–O–H angle of 150°; O–H stretching modes at 3963.7 cm⁻¹ (e, 2 × 296 km/mol), 3964.0 cm⁻¹ (b, 146 km/mol), and 3968.7 cm⁻¹ (a, 0 km/mol); and Zr–O stretching modes at 677.1 cm⁻¹ (a, 0 km/mol), 678.7 cm⁻¹ (b, 172 km/mol), and 689.7 cm⁻¹ (e, 2 × 243 km/mol).

Following the Hf(OH)₄ example, the major absorptions with the ¹⁶O₂ + ¹⁶O¹⁸O + ¹⁸O₂ reagent mixture are unshifted from the 3782.6 and 3770.7 cm⁻¹ pure isotopic positions, but the stronger new splittings at 3785.5 and 3772.2 cm⁻¹ are due to Zr(¹⁶OH)₂(¹⁸OH)₂, and these 2.9 and 1.5 cm⁻¹ splittings are in good agreement with calculated 2.9 and 1.9 cm⁻¹ splittings. The smaller splittings at 3784.4 and 3772.2 cm⁻¹ are due to Zr(¹⁶OH)₃(¹⁸OH) and Zr(¹⁶OH)(¹⁸OH)₃. Extra bands for the Zr–O stretching mode could not be found because of trace CO₂ and the Zr(¹⁶OH)₂ product between the major bands. The dominance of the strong 3782.4 cm⁻¹ band in the H₂O₂ experiments supports this assignment to the straightforward Zr-(OH)₄ reaction product.

The lower-symmetry Zr(OH)₂(OD)₂ molecule has four observable hydroxide modes, and as Table 4 shows, the antisymmetric O–H and O–D stretching modes are the same for Zr(OH)₄ and Zr(OD)₄, but weaker symmetric counterparts are predicted 2.5 and 3.5 cm⁻¹ higher, and these new bands are observed 2.4 and 3.4 cm⁻¹ higher at 3785.0 and 2796.0 cm⁻¹, respectively, in the mixed H₂O₂ + D₂O₂ experiment. The calculations predict the strongest Zr–O stretching modes 3.4 cm⁻¹ below this mode for Zr(OH)₄, and we observe this band 3.5 cm⁻¹ lower, and the next strongest at the position for Zr-(OD)₄, and we observe this band 0.5 cm⁻¹ higher. Again, the excellent agreement between observed and calculated frequencies, particularly those for the mixed isotopic molecules, confirms the identification of Zr(OH)₄.

The zirconium experiment with H₂ + D₂ + O₂ (Figure 5) gave the same new Zr(OH)₂(OD)₂ bands as found with H₂O₂ + D₂O₂. The Zr(OH)(OD)₃ molecule is also observed as an unresolved shoulder at 3782.6 cm⁻¹, and the Zr(OH)₃(OD) molecule also gives rise to a weak additional peak at 3786.0 cm⁻¹ for the symmetric O–H stretching mode. In addition,

stronger 2794.5 cm⁻¹ and weaker 2798.0 cm⁻¹ bands were observed for the O–D stretching mode of Zr(OH)₃(OD) and the symmetric O–D stretching mode of Zr(OH)(OD)₃, respectively. The quartet of bands observed at 2792.7, 2794.5, 2796.1, and 2798.0 cm⁻¹ reflects four different isotopic molecules containing O–D bonds, which are Zr(OD)₄, Zr(OH)₃(OD), Zr-(OH)₂(OD)₂, and Zr(OH)(OD)₃. Our observation of these four bands confirms that this is a tetrahydroxide species. The relative intensities of these four bands are qualitatively in agreement with calculated band intensities. Note that the antisymmetric O–D stretching modes of Zr(OH)₂(OD)₂, Zr(OH)(OD)₃, and Zr(OD)₄ all contribute to the strong 2792.7 cm⁻¹ absorption.

The above information is summarized in Figure 6, which represents the calculated product spectrum for 50/50 H/D substitution. The calculated O–H stretching frequencies are scaled by 3782.6/4048.1 = 0.9344, and the calculated O–D stretching frequencies are scaled by 2792.6/2950.4 = 0.9465. (These scale factors for strong t₂ modes show the slight difference in anharmonicity for the observed O–H and O–D stretching modes.) The calculated intensities (including degeneracies) are multiplied by the statistical weights for each Zr-(OH)ₓ(OD)ᵧ isotopic molecule (namely, 1, 4, 6, 4, and 2, all divided by 16) for x = 4, y = 0, represented as 4–0 in Figure 6, and for the 3–1, 2–2, 1–3, 0–4 molecules, respectively. This calculated spectrum matches the observed H₂ + D₂ + O₂ product spectrum (Figure 5h) very well.

The much weaker **d** bands with H₂O₂ are stronger relative to the **t** band with the H₂ + O₂ reagent. The **d** bands are 10.8 and 21.2 cm⁻¹ below the **t** bands, and our MP2 calculation for the ³B₁ ground-state Zr(OH)₂ molecule predicts the corresponding modes 23.8 and 30.1 cm⁻¹ lower than for Zr(OH)₄, which gives good agreement (Table 5). The upper **d** band exhibits the 1.00319 and 1.3546 ¹⁶O/¹⁸O and H/D isotopic ratios for an O–H stretching mode, and the lower band defines the 1.0387 ratio for ¹⁶O/¹⁸O that is lower than ZrO₂ itself, and the 22.1 cm⁻¹ D shift for this mode reveals H(D) participation. No shifts were observed for either band in the mixed isotopic experiments, which is in accord with frequency calculations. Our MP2 computation finds the ¹A₁ state 48 kcal/mol higher in energy. The B3LYP functional also predicts a ³B₁ ground state with a similar structure (angle O–Zr–O, 161.0°, angle Zr–O–H, 167.8°) with a 6 kcal/mol higher ¹A₁ state. A multireference calculation might be required for a better description of the triplet Zr(OH)₂ ground state.

Infrared spectra from the Zr/H₂O investigation[22] are shown in Figure 7. New bands appear at 3771.6 and 660.1 cm⁻¹ upon full arc photolysis, which increase upon annealing, and weaker 3782.3 and 681.6, 680.4 cm⁻¹ bands follow together upon annealing to 30 and 35 K. The 3771.6 cm⁻¹ band is clearly stronger than the 3782.3 cm⁻¹ absorption. These are the **t** and **d** bands observed with different relative intensities using H₂O
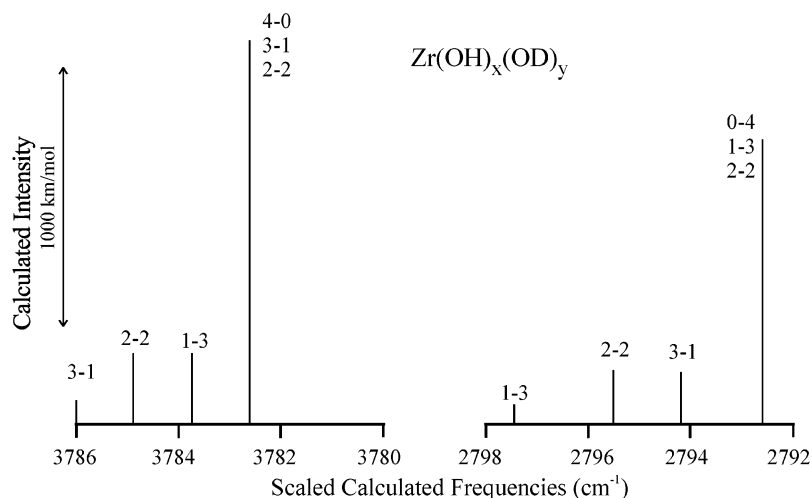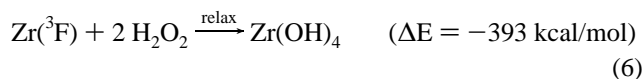
Figure 6. Calculated product spectrum for 50/50 H/D substitution for the zirconium experiment with $H_2 + D_2 + O_2$, confirming that the tetrahydroxide species has been preoduced.
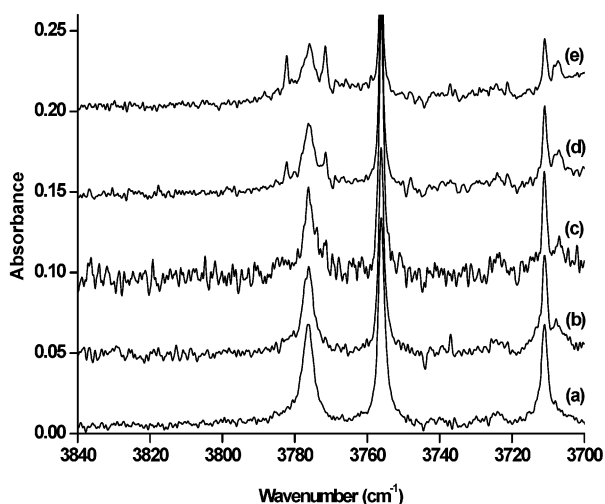
Figure 7. Infrared spectra of Zr atom and H_2O reaction products in excess argon at 11 K. (a) Sample deposition, (b) after annealing to 25 K, (c) after full-arc photolysis, (d) after annealing to 30 K, and (e) after annealing to 35 K.

compared to $H_2 + O_2$ and H_2O_2 as the reagent, and their association and observation from Zr and H_2O lends support to our assignments. Note that the **d** band is stronger than the **t** band using water, whereas the **t** bands are stronger than **d** using H_2O_2 and $H_2 + O_2$ reagents. We do not observe the 707.3 cm^{-1} band that Zhou et al.[22] associate with the 660.1 cm^{-1} absorption.

The spontaneous Zr reactions with H_2O_2 are almost as exothermic as those for Hf (B3LYP level). As for Hf(OH)$_4$, we find Zr(OH)$_4$ to be stable to decomposition in the gas phase, but the strongly exothermic heat of condensation of ZrO_2 (-212 kcal/mol) will favor decomposition in the solid phase.

$$Zr(^3F) + 2\,H_2O_2 \xrightarrow{\text{relax}} Zr(OH)_4 \qquad (\Delta E = -393\ \text{kcal/mol}) \tag{6}$$

$$Zr\,(^3F) + H_2O_2 \rightarrow Zr(OH)_2 \qquad (\Delta E = -194\ \text{kcal/mol}) \tag{7}$$

$$Zr(OH)_4 \rightarrow ZrO_2 + 2H_2O \qquad (\Delta E = 141\ \text{kcal/mol}) \tag{8}$$

Some comment on the photochemical reactions in the $H_2 + O_2$ systems is appropriate. We believe that the reaction mechanism involves first the formation of MO_2, which then inserts into H_2 to produce the dihydroxide (reaction 9), as has been

proposed for the group 2 systems.[9,10] The MO_2 and MH_2 molecules are both formed here. At this point, selectivity is lost, and other $H_2 + O_2$ reactions, including OH radical reactions, contribute to the overall $M(OH)_4$ product yield. We note that the Hf + HD + O_2 (Figure 2d) and Zr + H_2 + D_2 +O_2 (Figure 5h) product spectra have similar **t** band isotopic profiles, which verifies dihyrogen dissociation (and isotopic scrambling) in the overall reaction mechanism.

$$M + H_2 + O_2 \rightarrow MO_2 + H_2 \rightarrow M(OH)_2 \tag{9}$$
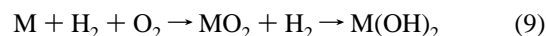
Several weak absorptions are probably due to the 23 kcal/mol more stable nonplanar HZr(O)OH isomer of $^3B_1$ ground-state Zr(OH)$_2$. Weak bands at 1539.6, 896.9, and 635.7 cm^{-1} with H_2O_2 (the latter are labeled **i** in Figure 4) increase upon early annealing along with the **d** bands, but they increase upon UV irradiation at the expense of the **d** bands. These bands shift to 1108.7, 896.5, and 622.4 cm^{-1} with D_2O_2, which is appropriate for Zr$-$H, Zr$=$O, and Zr$-$OH stretching modes. Our MP2 calculation for singlet, nonplanar HZr(O)OH predicts these modes at 1655.9, 880.6, and 672.0 cm^{-1}, and these bands are in reasonable agreement considering the approximation involved and using appropriate scaling.

$$Zr(OH)_2 \rightarrow HZr(O)OH \qquad (\Delta E = -23\ \text{kcal/mol, MP2}) \tag{10}$$
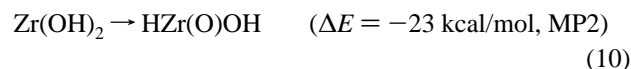
Finally, we calculated the trigonal Hf(OH)$_3$ and Zr(OH)$_3$ species, and both are stable structures (MP2: Hf$-$O, 1.949 Å; O$-$H, 0.953 Å; Zr$-$O, 1.954 Å; O$-$H, 0.954 Å). The strong O$-$H stretching modes fall between values for the $M(OH)_2$ and $M(OH)_4$ molecules, and we have no candidates for this assignment. The observation of the **d** bands as the second strongest absorption with H_2O_2 reagent evidences the dihydroxide assignment.

Titanium. Laser-ablated Ti atom reactions with H_2O_2 have very few product bands in common with two previous Ti/water investigations[22,31] because our most diagnostic activity is in the O$-$H stretching region, which is complicated by strong water absorption. We observe weak bands for TiO (987.8 cm^{-1}), TiO_2 (946.9, 917.1 cm^{-1}),[12] and HTiO (968.7 cm^{-1}),[22] and only the TiO_2 bands increase upon annealing. We also detect a very weak 1666.3 cm^{-1} band, which is the strongest feature previously assigned to $H_2Ti(OH)_2$.[22] Infrared spectra for H_2O_2 and D_2O_2 reactions are compared in Figure 8. In contrast to Hf and Zr,
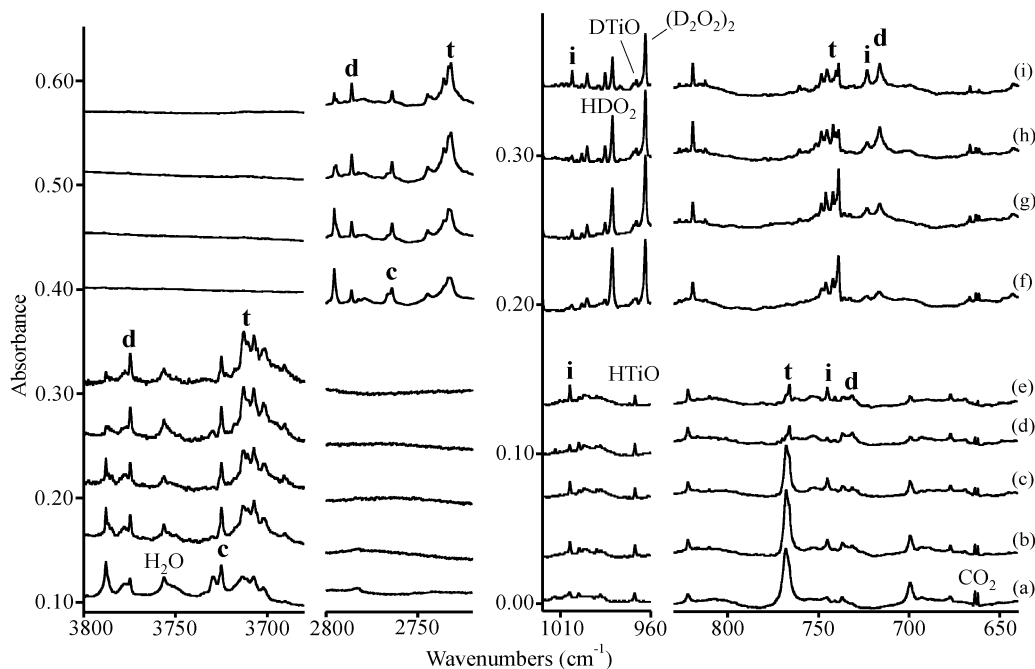
Figure 8. Infrared spectra of the Ti atom and H_2O_2 reaction products in excess argon at 10 K. (a) H_2O_2, (b) after annealing to 22 K, (c) after annealing to 26 K, (d) after $\lambda > 220$ nm irradiation, (e) after annealing to 30 K, (f) D_2O_2, (g) after annealing to 22 K, (h) after $\lambda > 220$ nm irradiation, and (i) after annealing to 34 K.
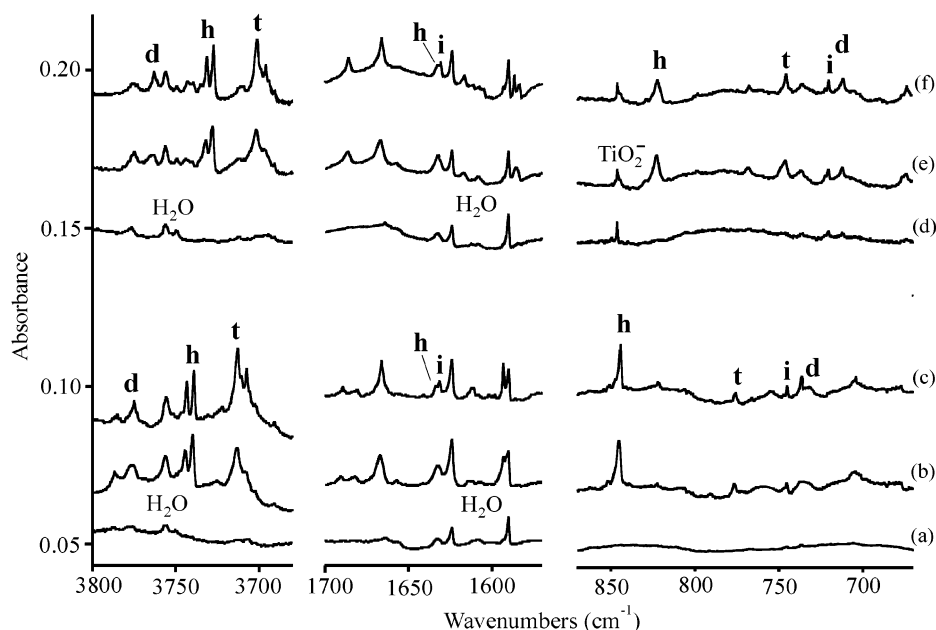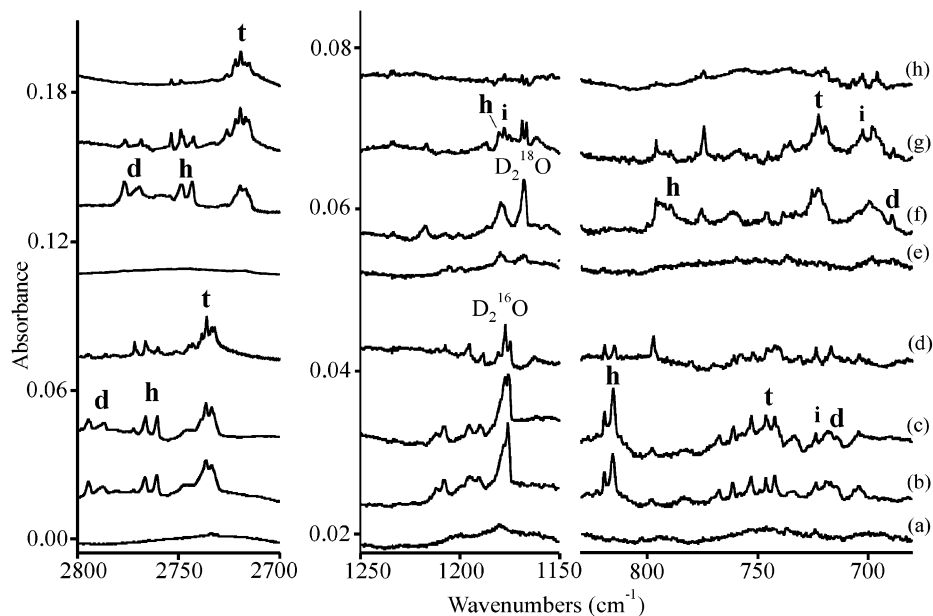

Figure 9. Infrared spectra of the Ti atom and $H_2 + O_2$ reaction products in excess argon at 10 K. (a) Sample deposited with $^{16}O_2$, (b) after $\lambda > 220$ nm irradiation, (c) after annealing to 20 K, (d) sample deposited with $^{18}O_2$, (e) after $\lambda > 220$ nm irradiation, and (f) after annealing to 19 K.

the Ti spectra exhibit two sharp upper bands, 3788.0 and 3774.7 cm^{-1}, with opposite annealing behavior and a multiplet at 3712.9 and 3707.3 cm^{-1} that increases upon annealing and photolysis. With D_2O_2, the sharp bands shift to 2795.4 and 2786.0 cm^{-1}, and the multiplet shifts to 2736.1, 2732.1 cm^{-1}. All hydrogen peroxide experiments share the HOH−O (3730.0, 3725.1 cm^{-1}) and DOD−O (2766.4, 2764.1 cm^{-1}) oxygen atom complex absorptions (labeled **c**),[18] as well as OH, OD, HO$_2$, and DO$_2$ radical absorptions,[24,25] which decrease on annealing. The lower-wavenumber region reveals new absorptions at 765.9, 745.1, 731.3, and 677.0 cm^{-1}, which shift to 746.2, 723.5, 716.6, and 666.8 cm^{-1} with D_2O_2.

Experiments with Ti, H_2, and O_2 produced some of the same and some new absorptions. Of course, TiO_2 bands were much

stronger, but TiH$_2$ (1435 cm^{-1}) was weak, and TiH$_4$ (1664 cm^{-1}) was not detected.[12,13] The uppermost bands were broader, now at 3786.7 and 3775.0 cm^{-1} in Figure 9, and the multiplet was almost the same, 3712.8, 3707.4 cm^{-1}, but two new sharper 3743.3, 3739.1 cm^{-1} features appeared upon UV irradiation. In the lower region, new bands were produced at 1685.8, 1662.2, 1637.5, 844.5, and 776.4 cm^{-1} upon UV irradiation. Spectra from the analogous experiment with $^{18}O_2$ substitution showed all bands shifted except those in the 1600 cm^{-1} region. Figure 10 illustrates spectra from the $D_2 + O_2$ and $D_2 + ^{18}O_2$ investigation, and counterpart product absorptions are listed in Table 3.

The Ti/H_2O spectra of Zhou et al.[22] were examined, and annealing increased sharp new 3743.5 and 3739.2 cm^{-1} bands

Figure 10. Infrared spectra of the Ti atom and $D_2 + O_2$ reaction products in excess argon at 10 K. (a) Sample deposited with $^{16}O_2$, (b) after $\lambda >$ 220 nm irradiation, (c) after annealing to 12 K, (d) after annealing to 24 K, (e) sample deposited with $^{18}O_2$, (f) after $\lambda >$ 220 nm irradiation, (g) after annealing to 22 K, and (h) after annealing to 30 K.

TABLE 6: Observed and Calculated Frequencies (cm^{-1}) for Ti(OH)$_4$ in the S_4 Structure ^{1}A State

mode	Ti(OH)$_4$ obs^a	Ti(OH)$_4$ calcd^b	Ti(OD)$_4$ obs	Ti(OD)$_4$ calcd	Ti(^{18}OH)$_4$ obs	Ti(^{18}OH)$_4$ calcd	Ti(^{18}OD)$_4$ obs	Ti(^{18}OD)$_4$ calcd
O−H stretch		3943.8 (a, 0)^c		2874.9 (0)		3930.4 (0)		2856.0 (0)
O−H stretch	3712.9	3935.2 (e, 428 × 2)	2736 .1	2865.6 (283 × 2)	3701. 3	3922.3 (414 × 2)	2719.4	2847.3 (267 × 2)
O−H stretch		3934.9 (b, 83)		2865.3 (64)		3922.0 (79)		2847.1 (58)
Ti−O stretch	765.9	799.5 (e, 319 × 2)	746. 2	778.8 (346 × 2)	744	775.3 (294 × 2)	725.6	755.1 (323 × 2)
Ti−O stretch		783.1 (b, 267)		769.3 (322)		757.3 (238)		744.1 (296)
Ti−O stretch		727.1 (a, 0)		708.2 (0)		688.8 (0)		670.7 (0)

^{a} Observed **t** bands in solid argon. ^{b} Calculated at the MP2/6-311++G(d,p)/SDD level. ^{c} Mode symmetry in S_4, infrared intensity (km/mol). ^{d} Additional frequencies calculated at 420 (192), 400 (0), 397 (162 × 2), 282 (250), 252 (0), 243 (155 × 2), 235 (45), 172 (80), 171 (10 × 2), 160 (0).

TABLE 7: Observed and Calculated Frequencies (cm^{-1}) for Ti(OH)$_2$ in the ^{3}B$_1$ State

mode	Ti(OH)$_2$ obs^a	Ti(OH)$_2$ calcd^b	Ti(OD)$_2$ obs	Ti(OD)$_2$ calcd	Ti(^{18}OH)$_2$ obs	Ti(^{18}OH)$_2$ calcd	Ti(^{18}OD)$_2$ obs	Ti(^{18}OD)$_2$ calcd
O−H stretch		4020.1 (a$_1$, 0)^c		2931.6 (0)		4006.5 (0)		2911.9 (0)
O−H stretch	3774. 7	4020.1 (b$_2$, 430)	2786.0	2929.6 (318)	3763.0	4006.6 (410)	2768.5	2910.5 (294)
Ti−O stretch	731.3	789.4 (b$_2$, 405)	716.6	775.6 (385)	711.8	764.7 (381)	689.3	753.3 (365)
Ti−O stretch		691.9 (a$_1$, 0)		671.1 (0)		654.0 (0)		636.9 (0)
Ti−O−H bend		458.2 (a$_2$, 0)		344.3 (0)		454.9 (0)		339.9 (0)
Ti−O−H bend		458.1 (b$_2$, 0)		344.2 (0)		455.8 (0)		339.8 (0)
Ti−O−H bend		420.4 (a$_1$, 194)		319.5 (105)		417.1 (192)		315.1 (103)
Ti−O−H bend		420.4 (b$_1$, 194)		319.3 (105)		417.1 (192)		314.9 (103)

^{a} Observed **d** bands in solid argon. ^{b} Calculated at the MP2/6-311++G(d,p)/SDD level. ^{c} Mode symmetry in C_{2v} although the molecule is essentially linear, infrared intensity (km/mol). The very small <17 cm^{-1} a$_1$ O−Zr−O bending frequency is omitted.

that track with the 844.3 cm^{-1} HTi(OH)$_3$ absorption and a 3707.8 cm^{-1} band on the side of water absorption. No 3788.0 and 3774.7 cm^{-1} absorptions were observed.

Comparison of the Ti/H$_2$O$_2$ spectra in Figure 8 with the Hf/H$_2$O$_2$ and Zr/H$_2$O$_2$ spectra in Figures 1 and 4 reveals a difference in the major product. The two higher-frequency absorptions at 3788.0 and 3774.7 cm^{-1} appear to be due to a single product, which we identify as Ti(OH)$_2$, in less and more stable matrix sites, respectively, and the major product bands at 3712.9 and 3707.3 cm^{-1} are assigned to Ti(OH)$_4$. Our MP2 and B3LYP calculations both predict the S_4 structure for Ti(OH)$_4$ and a triplet ground state for essentially linear Ti(OH)$_2$ with the singlet state 40 and 17 kcal/mol higher in energy, respectively. Of more importance, the triplet Ti(OH)$_2$ antisymmetric O−H stretching

frequency is predicted 85−100 cm^{-1} higher than that for Ti-(OH)$_4$. Hence, a reversal in the mode positions for the dihydroxides and tetrahydroxides is observed with Ti as compared to Hf and Zr. The observed and calculated frequencies for the titanium hydroxides are compared in Tables 6 and 7, and the agreement is satisfactory. A higher-level, possibly multiconfiguration calculation will be required for a more accurate description of the triplet Ti(OH)$_2$ ground-state molecule. We note that TiH$_2$ is computed to have a bent ^{3}B$_1$ ground state with several triplet states close in energy about 20 kcal/mol below the lowest singlet state.[32]

Another difference is that the third product is much stronger for Ti with both H$_2$O$_2$ and H$_2$ + O$_2$, which exhibits sharp absorptions at 1631.3, 1004.8, and 745.2 cm^{-1}. These bands

TABLE 8: Observed and Calculated Frequencies (cm^{-1}) for Singlet Ground-State HTi(O)OH

| mode | HTi(^{16}O)^{16}OH | | DTi(^{16}O)^{16}OD | | HTi(^{18}O)^{18}OH | | DTi(^{18}O)^{18}OD | |
	obs[a]	calcd[b]	obs	calcd	obs	calcd	obs	calcd
O−H stretch	*c*	3944.0 (196)	*c*	2873.2 (132)	*c*	3930.9	*c*	2854.6
Ti−H stretch	1631.3	1721.1 (382)	*d*	1233.2 (210)	1631.3	1721.1	1177.7	1232.9
Ti−O stretch	1004.8	1038.8 (98)	1003. 8	1036.6 (87)	964.3	995.8	962.4	993.5
Ti−O stretch	745.2	773.8 (196)	723.5	749.3 (204)	720.4	747.4	695.7	722.1
Ti−O−H bend		563.5 (34)		415.6 (16)		559.7		412.7
Ti−O−H bend		518.2 (166)		403.8 (97)		512.9		396.3
bend		468.3 (130)		374.2 (75)		461.4		366.2
bend		285.5 (153)		225.7 (36)		282.6		222.4
bend		207.2 (104)		176.2 (101)		201.2		173.5

[a] Observed bands in solid argon. [b] Calculated at the MP2/6-311++G(d,p)/SDD level. [c] Band probably masked by Ti(OH)$_4$ or Ti(OD)$_4$. [d] Band masked by D$_2$O.

increase together upon annealing, decrease together upon UV irradiation, and are restored upon final annealing to 30 K. These bands are in the regions for Ti−H, Ti=O, and Ti−O stretching frequencies, and the nonplanar HTi(O)OH isomer was computed in a singlet ground state and found to be 24 kcal/mol lower in energy than triplet Ti(OH)$_2$ at the MP2 level. (H out of O= Ti−OH plane; Ti−H, 1.733 Å; Ti=O, 1.623 Å; Ti−O, 1.815 Å; O−H, 0.960 Å; angles H−Ti−O, 117.9°; H−Ti=O, 106.1°; O=Ti−O, 112.8°; Ti−O−H, 137.3°). Table 8 lists the calculated and observed frequencies for four isotopic modifications, and the computed O−H stretching mode is unfortunately coincident with that for Ti(OH)$_4$. The sharp 1004.8 cm^{-1} band is 3.3% lower than the calculated Ti=O stretching mode, but of more importance, the observed and calculated small D and large ^{18}O isotopic shifts match very well (Table 8). The sharp 745.2 cm^{-1} band is 3.7% lower than the calculated Ti−O stretching mode, and again, the observed and calculated isotopic shifts are in good agreement. Next, the calculated Ti−H stretching mode at 1721.1 cm^{-1} is 5.2% higher than the sharp new 1631.3 cm^{-1} absorption, which shows the proper isotopic shifts for this mode. Finally, it is interesting to note that the HTi(O)OH isomer is more photosensitive than Ti(OH)$_2$, although the more stable isomer is favored upon final annealing, and that this tetravalent "dihydroxide" isomer is more stable for Ti > Zr > Hf based on relative product yields in H$_2$O$_2$ experiments.

The strong new bands (labeled **h**) at 3739.1 and 3743.3 cm^{-1} with H$_2$ + O$_2$ (Figure 9) track with the 1634 and 844 cm^{-1} absorptions previously assigned to HTi(OH)$_3$ by Zhou et al.[22] The latter stronger absorption was also observed by Kaufmann et al.,[31] who reported a mixed H/D isotopic pentet. First, our 3739.1 and 3743.3 cm^{-1} absorptions shift to 3727.3 and 3731.3 cm^{-1} with ^{18}O$_2$ (ratio = 1.00324, 1.00317), to 2760.1 and 2766.3 cm^{-1} with D$_2$ (ratio = 1.3547, 1.3533), and to 2742.6 and 2748.9 cm^{-1} with D$_2$ + ^{18}O$_2$. These ratios are indicative of an O−H (O−D) stretching mode.

We computed HTi(OH)$_3$ at the MP2 level and found a singlet C_3 structure with strong e stretching modes predicted at 3950 and 855 cm^{-1}. We also calculated the eight mixed H/D isotopic molecules, and the strong 855 cm^{-1} mode does become a pentet absorption like that reported by Kaufmann et al.[31] Our H$_2$ + ^{18}O$_2$ spectrum has sufficient ^{16}O$_2$ impurity to give mixed ^{16}O/ ^{18}O oxygen absorptions appropriate for this degenerate mode.

The two associated absorptions at 822.0 (819.4) and 677.0 (666.8) cm^{-1} with Ti and H$_2$O$_2$ (D$_2$O$_2$) cannot be identified. As these absorptions are produced only with hydrogen peroxide, we do not have ^{18}O$_2$ data. The 819.4 cm^{-1} band clearly shows Ti isotopic subpeaks at 826.8, 823.0, 816.2, and 812.6 cm^{-1}, which indicates slightly more participation of a single Ti atom than observed for TiO$_2$.[12] Both absorptions fall in the generic
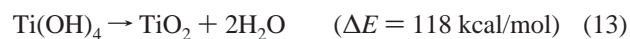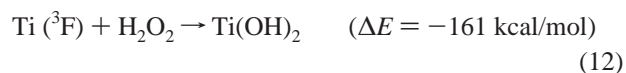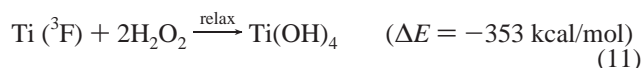
TABLE 9: Mulliken Charges Computed for Metal Hydroxide Molecules[a]

molecule[b,c]	q (M)	q (O)	q (H)	ν(O−H)[d]
Ba(OH)$_2$	1.66	−1.25	0.42	3724
Hf(OH)$_2$ (^{1}A$_1$)	0.58	−0.75	0.46	3789
Hf(OH)$_4$	1.43	−0.75	0.39	3796
Sr(OH)$_2$	1.75	−1.36	0.49	3761
Zr(OH)$_2$ (^{3}B$_1$)	0.70	−0.70	0.35	3772
Zr(OH)$_4$	2.24	−0.93	0.37	3783
Ca(OH)$_2$	1.72	−1.34	0.48	3785
Ti(OH)$_2$ (^{3}B$_1$)	1.12	−0.94	0.38	3775
Ti(OH)$_4$	0.36	−0.38	0.29	3707

[a] Calculated at the MP2/6-311++G(d,p)/SDD level. [b] Group 2 molecules from ref 10. [c] Structures in Figure 3. [d] Argon matrix frequency (cm^{-1}). Different Ti(OH)$_2$ matrix site absorption at 3788 cm^{-1}.

Ti−O stretching region. We have performed a number of calculations in an attempt to identify this molecule without success.

The spontaneous reactions of Ti with H$_2$O$_2$ are almost as exothermic as those of Zr (B3LYP level). We find Ti(OH)$_4$ to be stable but less so toward decomposition in the gas phase, and the strongly exothermic heat of condensation computed from heats of formation[30] and our TiO$_2$ energy (−171 kcal/mol) favor decomposition in the solid phase.

$$\text{Ti (}^3\text{F)} + 2\text{H}_2\text{O}_2 \xrightarrow{\text{relax}} \text{Ti(OH)}_4 \qquad (\Delta E = -353 \text{ kcal/mol}) \tag{11}$$

$$\text{Ti (}^3\text{F)} + \text{H}_2\text{O}_2 \rightarrow \text{Ti(OH)}_2 \qquad (\Delta E = -161 \text{ kcal/mol}) \tag{12}$$

$$\text{Ti(OH)}_4 \rightarrow \text{TiO}_2 + 2\text{H}_2\text{O} \qquad (\Delta E = 118 \text{ kcal/mol}) \tag{13}$$

Group 2 and 4 Comparisons. Mulliken charges, which are overestimates of the charge distribution in the molecule, for the hydroxides are compared in Table 9. The charges on the Group 4 metals are all less than those on their adjacent group 2 metals, as expected from ionization energies,[30] but this difference is less so for Ti and Ca. The dihydroxide frequency is 65 cm^{-1} lower for Ba than for Hf, but only 11 cm^{-1} lower for Sr than Zr, and the Ca(OH)$_2$ frequency falls between two matrix site frequencies for Ti(OH)$_2$. The O−H stretching frequency itself is not a measure of ionic character as the OH (3569 cm^{-1}) and OH$^-$ (3556 cm^{-1}) frequencies are almost the same.[29,33]

Differences in the Group 4 tetrahydroxides are more striking. The charge on Ti is far less than those on Zr and Hf, and Ti-(OH)$_4$ has bent Ti−O−H bonds and the S_4 structure, suggesting more covalent character.[28] The recently prepared Pb(OH)$_4$ molecule, which is also more covalent, shares the S_4 structure, bent M−O−H bonds, and low O−H stretching frequency (3608

Spectra and Structures for Group 4 Di- and Tetrahydroxides

J. Phys. Chem. A, Vol. 109, No. 47, 2005 **10701**

cm^{-1}).[34] On the other hand, the ionic Zr(OH)$_4$ molecule is even more ionic than Hf(OH)$_4$, consistent with the slightly lower ionization energy of Zr compared to Hf.[30] Finally, Zr(OH)$_4$ and Hf(OH)$_4$ are computed to be very stable tetrahedral molecules.

Conclusions

Hafnium and zirconium atoms react with H$_2$O$_2$ and with H$_2$ + O$_2$ mixtures in solid argon to form the M(OH)$_2$ and M(OH)$_4$ molecules, which are identified from matrix infrared spectra with the assistance of isotopic substitution. Electronic structure calculations at the MP2 level predict almost linear and tetrahedral molecules, respectively, and frequencies for mixed isotopic molecules of lower symmetry that are in excellent agreement with observed values, which confirms the identification of these hafnium and zirconium dihydroxide and tetrahydroxide molecules. In particular, the observation of resolved O−D stretching modes for the four isotopic molecules M(OH)$_3$-(OD), M(OH)$_2$(OD)$_2$, M(OH)(OD)$_3$, and M(OD)$_4$ for Hf and Zr conclusively identifies these tetrahydroxide molecules. Our observations show that these structures are tetrahedral or nearly tetrahedral. Titanium reacts to give the same products, but Ti-(OH)$_4$ has the S_4 structure with bent Ti−O−H bonds, and Ti-(OH)$_2$ appears to be nearly linear. This work reports definitive evidence for Group 4 dihydroxides and tetrahydroxides, which are the first examples of metal tetrahydroxide molecules.

References and Notes

(1) Cotton, F. A.; Wilkinson, G.; Murillo, C. A.; Bochmann, M. *Advanced Inorganic Chemistry*, 6th ed.; Wiley: New York, 1999.
(2) (a) Wells, A. F. *Structural Inorganic Chemistry*, 4th ed.; Clarendon Press: Oxford, U.K., 1975. (b) McWhan, D. B.; Lundgren, G. *Inorg. Chem.* **1966**, *5*, 284. (c) Hansson, M. *Acta Chem. Scand.* **1969**, *23*, 3541. (d) See also Inorganic Crystal Structure Database at http://icsd.ill.fr/icsd/.
(3) Greenwood, N. N.; Earnshaw, A. *Chemistry for the Elements*, 2nd ed.; Butterworth-Heinemann: Oxford, U.K. 1997.
(4) Holleman, A. F.; Wiberg, E. *Lehrbuch der Anorganischen Chemie*; Wiberg, N., Ed.; Walter de Gruyter: Berlin, 1995; Vol. 101.
(5) Higgins, K. J.; Fruend, S. M.; Klemperer, W.; Apponi, A. J.; Ziurys, L. M. *J. Chem. Phys.* **2004**, *121*, 11715.
(6) Li, M.; Coxon, J. A. *J. Chem. Phys.* 1995, *102*, 2663; **1996**, *104*, 4961 and references therein.
(7) Whitham, C. J.; Ozeki, H.; Saito, S. *J. Chem. Phys.* **2000**, *112*, 641 and references therein.
(8) Lakin, N. M.; Varberg, T. D.; Brown, J. M. *J. Mol. Spectrosc.* **1997**, *183*, 34.
(9) Andrews, L.; Wang, X. *Inorg. Chem.* **2005**, *44*, 11.
(10) Wang, X.; Andrews, L. *J. Phys. Chem. A* **2005**, *109*, 2782.
(11) Wang, X.; Andrews, L. *J. Phys. Chem. A* **2005**, *109*, 3849.
(12) Chertihin, G. V.; Andrews, L. *J. Phys. Chem.* **1995**, *99*, 6356.
(13) Chertihin, G. V.; Andrews, L. *J. Am. Chem. Soc.* **1995**, *117*, 6402.
(14) Chertihin, G. V.; Andrews, L. *J. Phys. Chem.* **1995**, *99*, 15004.
(15) Siegbahn, P. E. M.; Bloomberg, M. R. A.; Svensson, M. *J. Am. Chem. Soc.* **1993**, *115*, 4191.
(16) Wang, X.; Andrews, L. *Inorg. Chem.* **2005**, *44*, 7189.
(17) Andrews, L. *Chem. Soc. Rev.* **2004**, *33*, 123 and references therein.
(18) (a) Pettersson, M.; Tuominen, S.; Rasanen, M. *J. Phys. Chem. A* **1997**, *101*, 1166. (b) Pehkonen, S.; Pettersson, M.; Lundell, J.; Khriachtchev, L.; Rasanen, M. *J. Phys. Chem. A* **1998**, *102*, 7643.
(19) Frisch, M. J.; Trucks, G. W.; Schlegel, H. B.; Scuseria, G. E.; Robb, M. A.; Cheeseman, J. R.; Zakrzewski, V. G.; Montgomery, J. A., Jr.; Stratmann, R. E.; Burant, J. C.; Dapprich, S.; Millam, J. M.; Daniels, A. D.; Kudin, K. N.; Strain, M. C.; Farkas, O.; Tomasi, J.; Barone, V.; Cossi, M.; Cammi, R.; Mennucci, B.; Pomelli, C.; Adamo, C.; Clifford, S.; Ochterski, J.; Petersson, G. A.; Ayala, P. Y.; Cui, Q.; Morokuma, K.; Malick, D. K.; Rabuck, A. D.; Raghavachari, K.; Foresman, J. B.; Cioslowski, J.; Ortiz, J. V.; Stefanov, B. B.; Liu, G.; Liashenko, A.; Piskorz, P.; Komaromi, I.; Gomperts, R.; Martin, R. L.; Fox, D. J.; Keith, T.; Al-Laham, M. A.; Peng, C. Y.; Nanayakkara, A.; Gonzalez, C.; Challacombe, M.; Gill, P. M. W.; Johnson, B.; Chen, W.; Wong, M. W.; Andres, J. L.; Gonzalez, C.; Head-Gordon, M.; Replogle, E. S.; Pople, J. A. *Gaussian 98*, revision A.6, Gaussian, Inc.: Pittsburgh, PA, 1998 and references therein.
(20) Frisch, M. J.; Pople, J. A.; Binkley, J. S. *J. Chem. Phys.* **1984**, *80*, 3265.
(21) Andrae, D.; Haeussermann, U.; Dolg, M.; Stoll, H.; Preuss, H. *Theor. Chim. Acta* **1990**, *7*, 123.
(22) Zhou, M. F.; Zhang, L. N.; Dong, J.; Qin, Q. Z. *J. Am. Chem. Soc.* **2000**, *122*, 10680.
(23) (a) Langford, V. S.; McKinley, A. J.; Quickenden, T. I. *J. Am. Chem. Soc.* **2000**, *122*, 12859. (b) Cooper, P. D.; Kjaergaard, H. G.; Langford, V. S.; McKinley, A. J.; Quickenden, T. I.; Schofield, D. P. *J. Am. Chem. Soc.* **2003**, *125*, 6048.
(24) (a) Milligan, D. E.; Jacox, M. E. *J. Chem. Phys.* **1963**, *38*, 2627. (b) Smith, D. W.; Andrews, L. *J. Chem. Phys.* **1974**, *60*, 81.
(25) Cheng, B.-M.; Lee, Y.-P.; Ogilvie, J. F. *Chem. Phys. Lett.* **1988**, *109*, 151.
(26) Scott, A. P.; Radom, L. *J. Phys. Chem.* **1996**, *100*, 16502.
(27) Kaupp, M.; Schleyer, P. v. R. *J. Am. Chem. Soc.* **1992**, *114*, 491.
(28) Ikeda, S.; Nakajima, T.; Hirao, K. *Mol. Phys.* **2003**, *101*, 105.
(29) Rosenbaum, N. H.; Owrutsky, J. C.; Tack, L. M.; Saykally, R. J. *J. Chem. Phys.* **1986**, *84*, 5308.
(30) Selected Values of Chemical Thermodynamic Properties. In *CRC Handbook of Chemistry and Physics*, 66th ed.; Weast, Robert C., Ed.; CRC Press: Boca Raton, FL, 1985; p D-89.
(31) Kauffman, J. W.; Hauge, R. H.; Margrave, J. L. *J. Phys. Chem.* **1985**, *89*, 3547.
(32) Kudo, T.; Gordon, M. S.; *J. Chem. Phys.* **1995**, *102*, 6806.
(33) Huber, K. P.; Herzberg, G. *Molecular Spectra and Molecular Structure*; Van Nostrand Reinhold: New York, 1979; Vol. IV, Constants of Diatomic Molecules.
(34) Wang, X.; Andrews, L. *J. Phys. Chem. A* **2005**, *109*, 9013.